ACS APPLIED MATERIALS & INTERFACES

RESEARCH ARTICLE

www.acsami.org

Synthesis of β-Mo_2C Thin Films

Colin A. Wolden,*[,†] Anna Pickerell,[†] Trupti Gawai,[†] Sterling Parks,[†] Jesse Hensley,[‡] and J. Douglas Way[†]

[†]Department of Chemical Engineering, Colorado School of Mines, Golden, Colorado 80401, United States

[‡]National Renewable Energy Laboratory, 1617 Cole Boulevard, Golden, Colorado 80401, United States

ABSTRACT: Thin films of stoichiometric β-Mo_2C were fabricated using a two-step synthesis process. Dense molybdenum oxide films were first deposited by plasma-enhanced chemical vapor deposition using mixtures of MoF_6, H_2, and O_2. The dependence of operating parameters with respect to deposition rate and quality is reviewed. Oxide films 100−500 nm in thickness were then converted into molybdenum carbide using temperature-programmed reaction using mixtures of H_2 and CH_4. X-ray diffraction confirmed that molybdenum oxide is completely transformed into the β-Mo_2C phase when heated to 700 °C in mixtures of 20% CH_4 in H_2. The films remained well-adhered to the underlying silicon substrate after carburization. X-ray photoelectron spectroscopy detected no impurities in the films, and Mo was found to exist in a single oxidation state. Microscopy revealed that the as-deposited oxide films were featureless, whereas the carbide films display a complex nanostructure.

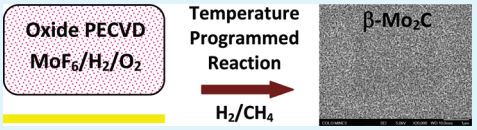

KEYWORDS: thin film, carbide, oxide, plasma-enhanced chemical vapor deposition, catalyst

INTRODUCTION

Molybdenum carbide is a versatile material with potential applications in a variety of areas. Molybdenum carbide exhibits catalytic properties analogous to platinum group metals, and in the last few decades, efforts have been made to exploit this trait in a number of chemical processes including ammonia synthesis, hydrocarbon reforming, water gas shift, H_2 production, and alcohol synthesis.[1−7] As a thin film, the high hardness and thermal stability of the transition metal carbides make them useful as wear-resistant materials.[8,9] More recent studies have focused on the optoelectronic properties of molybdenum carbide for a range of applications including mirrors,[10] diffusion barriers,[11] interconnects,[12] and electron field emission.[13] Our interest is in the creation of inexpensive alternatives to platinum group metals for surface dissociation of H_2. Formation of this material as a thin film would facilitate fundamental studies of catalyst performance.

Numerous techniques have been used to deposit molybdenum carbide films including chemical vapor deposition (CVD),[8,14] physical vapor deposition (PVD),[9,11] and electrodeposition.[15] The Mo−C system is quite complex, with numerous stable and metastable compounds and crystal phases that have been observed.[14,16] Control of phase purity has been problematic for both CVD and PVD approaches, and films often contain a mixture of carbon-rich products that display a complex dependence on the specific operating conditions employed.[8,11,14] In contrast, for catalysis applications it is relatively straightforward to achieve the desired β-Mo_2C phase in powder form.[1−4] The key development came from Boudart and coworkers[1,2] who developed a method to convert dense MoO_3 powders into high-surface-area Mo_2C by temperature-programmed reaction or TPR, using mixtures of hydrocarbons diluted in H_2. The mechanism for the MoO_3 to Mo_2C transformation involves the substitution of carbon for oxygen in the MoO_3 lattice, with little displacement of the Mo atoms during the reaction. Because the molar volume of Mo_2C is smaller than the molar volume of MoO_3, micropores form as the oxide transforms into the carbide. Under proper conditions the MoO_3 is converted into Mo_2C without forming metallic Mo as a reaction intermediate. Metal sintering is avoided using this method, and unsupported catalysts can be prepared with very high surface areas (50−90 m^2/g). Rebrov et al.[5] used this strategy to form catalyst coatings through the carburization of pre-oxidized molybdenum sheets, and applied them to the water gas shift reaction.

The goal of this work was to produce phase pure β-Mo_2C films for future study as model catalyst layers. Below we describe a two-step synthesis approach. First, dense molybdenum oxide films are deposited on silicon using plasma-enhanced chemical vapor deposition (PECVD) using mixtures of $MoF_6/H_2/O_2$. The use of MoF_6 and this reaction chemistry is somewhat unique, as previous CVD of Mo-containing compounds have employed either $Mo(CO)_6$[17,18] or $MoCl_5$[14,19] as the molybdenum precursor. The dependence of oxide growth rate and quality on PECVD parameters is described. The use of PECVD to form the oxide allows these films to be produced on a broader set of substrates. The films were then transformed into the β-Mo_2C phase by applying TPR conditions developed by the catalysis community. The evolution of film composition and structure throughout these processes is quantified using a suite of analytical techniques.

EXPERIMENTAL SECTION

Oxide Synthesis. Molybdenum oxide films were deposited using mixtures of $MoF_6/H_2/O_2$ in a capacitively-coupled PECVD system. This PECVD chemistry adopts a similar approach that has been

Received: November 11, 2010
Accepted: December 31, 2010
Published: January 20, 2011

successfully applied for the synthesis of electrochromic WO_3 films using analogous gas mixtures ($WF_6/H_2/O_2$).[17,20] Molybdenum hexafluoride (Acros Organic, 99.5 vol %) decomposes readily, however the reaction is reversible as the released fluorine radicals will etch the film. To mitigate this issue, we add hydrogen to scavenge atomic fluorine, forming HF. Oxygen is also supplied in excess to ensure fully oxidized films. All depositions described here were conducted at ambient temperature with the plasma power fixed at 200 W. MoF_6 was delivered using a calibrated needle valve, whereas electronic mass flow controllers were used for O_2 and H_2 flow rates. The reactor was pumped using a Fomblin-equipped mechanical pump (Edwards, E2M40) with deposition pressures in the range of 500−700 mTorr depending on total flow rate.

Carburization. The carburization process was conducted by TPR in a temperature-controlled flowtube using conditions adopted from the literature.[1,2] Initial studies employed commercial MoO_3 powders (Sigma-Aldrich, 99.5%) to verify the efficacy of the process. Approximately 1 g of powder was placed in a crucible, inserted into the flowtube, and calcined using 200 sccm of bone dry air at 500 °C for an hour to desorb any moisture. The gas was then switched to a 20 vol. % CH_4/H_2 mixture at a total flow rate of 400 sccm, and the temperature was ramped at a rate of 1° C/min up to 700 °C, where it was held for 3 h. After carburization, the furnace was turned off and samples were cooled to room temperature under the flow of industrial grade nitrogen, which also served to passivate the carbide prior to exposure to air. Oxide films were transformed into the molybdenum carbide using the identical procedure.

Characterization. Spectroscopic ellipsometry (SE, J. A. Woollam) was used to determine the oxide film thickness and refractive index of the as-deposited films. All indices of refraction are taken at 580 nm. Measurements were taken at an angle of 70°, and data was collected over the range of 400 -1300 nm. X-ray diffraction (XRD, Siemens Kristalloflex 810) was performed using a Cu Kα radiation source to determine the growth orientation of the thin films using a scan rate of 3°/min with a step size of $2\theta = 0.05$. X-ray photoelectron spectroscopy (XPS, Kratos) was performed ex situ using an Al Kα X-ray source. The base pressure of the analysis chamber was $<1 \times 10^{-9}$ Torr, and high-resolution spectra of individual binding states were recorded using a scan time of 60 seconds at a pass voltage of 40 eV. The binding energy scale was calibrated by positioning the adventitious C 1s peak at 284.6 eV,[21] and in the figures below spectra are offset for clarity. Samples were examined both as-received and after an Ar ion sputter treatment. The sputter cleaning time was set at 2 min, which was found to be the minimum time required to remove adventitious carbon. Information on film morphology and surface roughness was obtained by field-emission scanning electron microscopy (FESEM, JEOL JSM-7000F) and by atomic force microscopy (AFM, Digital Instruments Nanoscope III) operated in tapping mode.

RESULTS AND DISCUSSION

Molybdenum Oxide Synthesis. The trends observed in this work are nominally identical to those reported previously for PECVD synthesis of WO_3 from $WF_6/H_2/O_2$.[20] The deposition rate scales to first order with MoF_6 flow rate, and this value was fixed at 5 sccm for the resulted reported here. Important values for optimizing rate and quality are the ratios between the precursor and its co-reagents O_2 and H_2. Figure 1 displays the effect of these parameters on deposition rate and refractive index. First, note that oxygen is supplied in great excess in all experiments. The rate was relatively insensitive to O_2 at ∼40 nm/min, declining slightly as the ratio is increased (Figure 1a). Refractive index measurements can be taken to be an indication of film density, and it has been shown that high values have been correlated with low hydrogen content.[22] The refractive index at

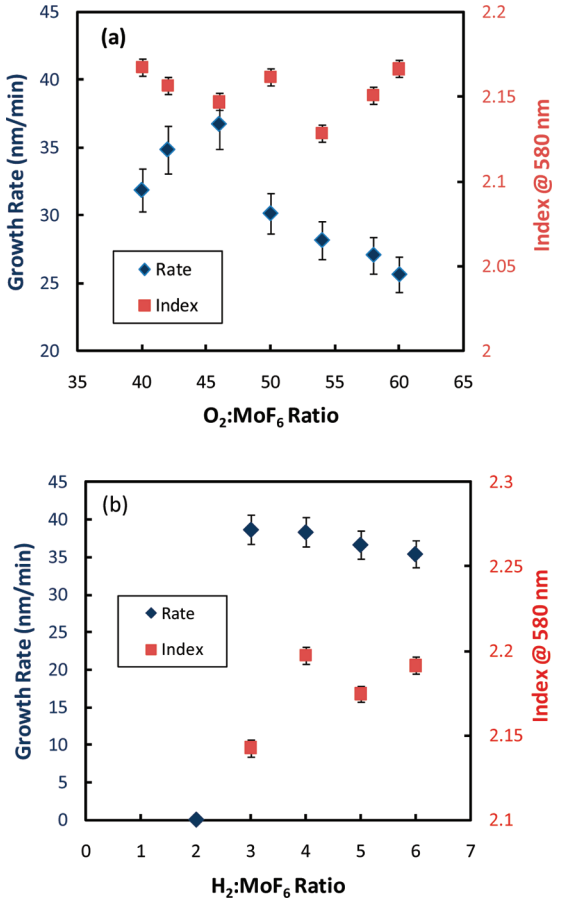

Figure 1. Graphs showing the dependence of molybdenum oxide growth rate (left axis) and refractive index (right) as a function of (a) O_2:MoF_6 ratio and (b) H_2:MoF_6 ratio.

580 nm is essentially unchanged at a value of ∼2.2, and this value is among the highest values reported in the literature for as-deposited films.[23] This indicates that O_2 is being supplied in sufficient excess.

In contrast, the rate and quality are quite sensitive to the H_2:MoF_6 ratios. Note that continuous, well-adhered films could not be formed with H_2:MoF_6 ratios less than 3. At sub-stoichiometric ratios appreciable concentrations of atomic F are present, which is deleterious to film growth. When supplied in excess the H_2 will react with O_2 to form water or possibly be incorporated in the film as MoO_3:H, which results in an electrochromic response. Films discussed below were deposited using ratios of O_2:MoF_6 = 50 and H_2:MoF_6 = 4.

XPS was used to further examine the composition and bonding within the as-deposited films. One concern with the use of MoF_6 as a precursor is the possibility of fluorine incorporation. Figure 2 displays high-resolution spectra of the F1 s core region. A small amount of fluorine is detected on the surface of the as-deposited film. However it is completely removed using the Ar^+ sputter clean, and no F is detectable within the films. The film composition was further examined by looking at the Mo 3d region, which is shown in Figure 3. The spectra in Figure 3 were obtained without sputter cleaning, since molybdenum oxide is substantially reduced by this process. The Mo signal is split into the Mo $3d_{5/2}$ and Mo $3d_{3/2}$ doublet caused by spin-orbit coupling.[24] Table I summarizes the location of the Mo $3d_{5/2}$ signal reported in the literature for various oxidation states.[4,8,21,25,26]

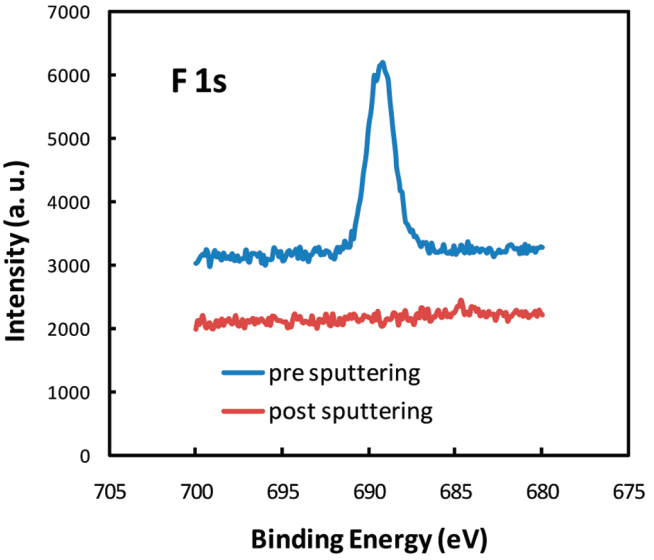

Figure 2. High-resolution XPS spectra of the F 1s region obtained from an as-deposited MoO_3 films and after sputter cleaning.

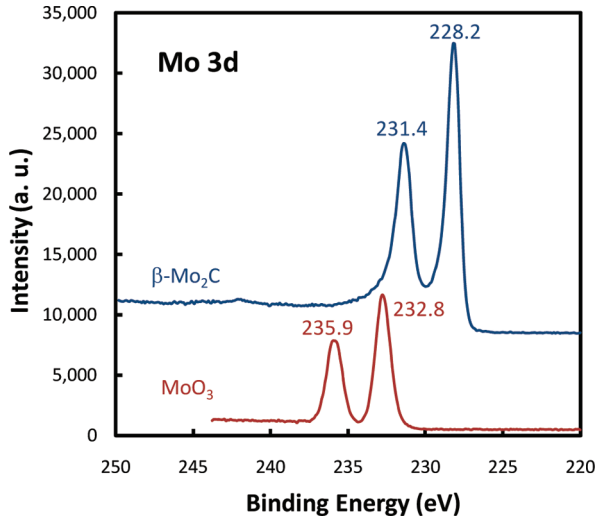

Figure 3. High-resolution XPS spectra of the Mo 3d region obtained from an as-deposited MoO_3 film, and after carburization.

The observed peak position of the as-deposited film at a binding energy (BE) of 232.8 eV is in good agreement with the Mo^{+6} state of fully oxidized MoO_3. The d orbital peaks are separated by 3.1 eV and appear in the theoretically expected 3:2 ratio,[24] providing further support that the Mo is present in a single oxidation state. Of course hydrogen cannot be detected by XPS, but the position of Mo spectra in its fully oxidized state supports its absence. XPS analysis of molybdenum oxide films intercalated with H display the presence of Mo^{+5} and Mo^{+4} oxidation states.[21] Moreover, the transparent nature of the film provide further support for its chemical purity, since MoO_3H_x has a grey color that is exploited in electrochromic applications.[21,27]

Carburization. Molybdenum oxide films with thickness of 100−500 nm were deposited on pieces of (100) silicon wafers as described above. These samples were then carburized using standard TPR conditions described above. Films remained well-adhered to the underlying silicon substrate after carburization,

Table I. Summary of the Binding Energy Positions Reported in the Literature (± 0.2 eV) for the Mo $3d_{5/2}$ and C 1s Core Levels in Oxidation States of Interest to Mo_2C Formation

state	BE (eV)
Mo^{6+}	232.9
Mo^{5+}	231.8
Mo^{4+}	229.9
Mo^{3+}	228.8
Mo^{2+}	228.2
Mo^{0}	227.6
Carbide C	283.0
Graphitic C	284.5

and were characterized using the techniques described below. The changes in crystal structure that were observed in conjunction with TPR are summarized in Figure 4, which compares results from both powder samples and a 200 nm thick film with literature standards. The stable phase of molybdenum oxide has an orthorhombic structure,[27] and the as-received powders were in good agreement with the literature standards (JCPDS 76-1003).

The as-deposited oxide films are XRD amorphous, however they crystallize when annealed in air at temperatures >150 °C. During the carburization process, the oxide films are transformed during the calcining step, and an example of a XRD pattern obtained from a film after this treatment is shown in Figure 4. The pattern obtained from the thin film sample is noisy relative to the powder samples, but nevertheless the film is clearly identified as polycrystalline molybdenum oxide with a preferential orientation in the (110) direction located at $2\theta = 23.33°$.

The same materials were examined after the completion of the carburization process. Again it is observed that the powder samples are in perfect agreement with literature expectations for the β-Mo_2C phase. Note that the β-Mo_2C phase has an orthorhombic crystal structure (JCPDS 79-0744), though its lattice positions are nominally identical to a slightly strained hexagonal closed packed structure (JCPDS 35-0787), and it has often been described as such in the catalyst literature.[16,28] Both carbide powders and films display the three significant peaks at 2θ of 34.4, 37.9, and 39.4 which are indexed as the (100), (002), and (101) planes of β-Mo_2C, respectively. There is no evidence of residual oxide, molybdenum metal, or any other crystalline phases of molybdenum carbide. The XRD pattern obtained from a carburized film is nominally identical to both the literature values and the powder sample, confirming its transformation to the β-Mo_2C phase.

XPS was used to examine the composition of the carburized films. Figure 3 contains the high resolution spectra of Mo 3d region. The position of the Mo peaks in the carbide was shifted significantly to lower binding energy relative to the oxide film, and the peak position at BE = 228.2 eV is in perfect agreement with literature values for Mo^{+2} (Table I). The compositional purity of this material is again supported by both the spacing (3.2 eV) and relative intensity of the two peaks, which suggests that the Mo is predominantly in a single oxidation state. Figure 5 compares high resolution spectra of the O 1s region obtained from an oxide film and after carburization. The oxide film displays a prominent peak at BE = 530.8 eV, which is in good agreement with literature values.[29] The surface of the carbide is partially oxidized during the passivation step. Although the signal is attenuated substantially relative to the oxide film, there are two

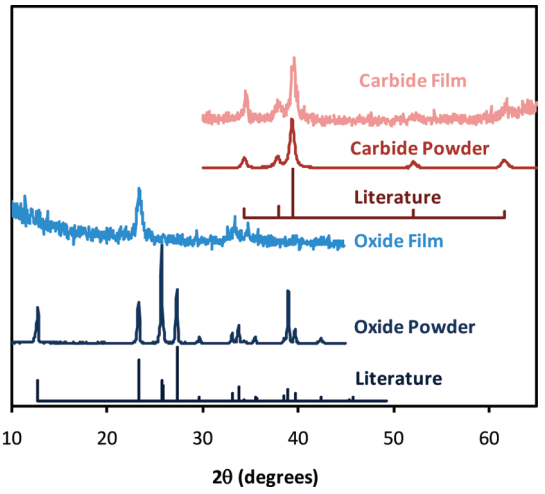

Figure 4. Comparison of XRD patterns obtained from oxide powder and a 200 nm oxide film before (bottom) and after (top) the TPR carburization process. Literature values obtained from JCPDS 76-1003 (oxide) and JCPDS 79-0744 (carbide).

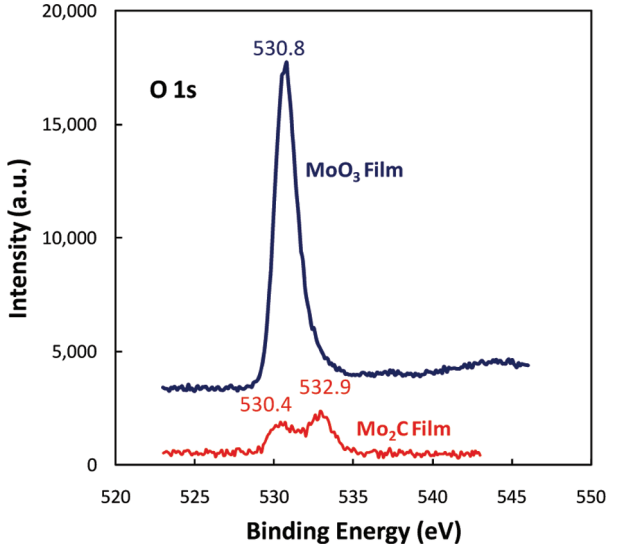

Figure 5. High-resolution XPS spectra of the O 1s region obtained from an as-deposited MoO_3 film, and after carburization.

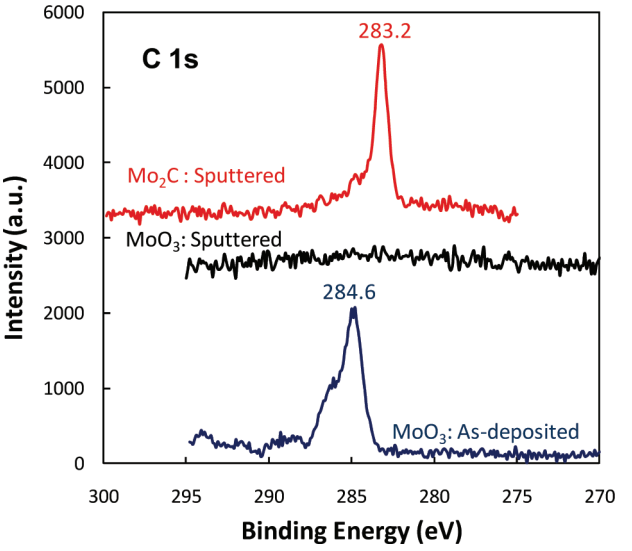

Figure 6. High-resolution XPS spectra of the C 1s region obtained from an as-deposited MoO_3 film, after sputter cleaning, and a Mo_2C film after the identical sputter treatment.

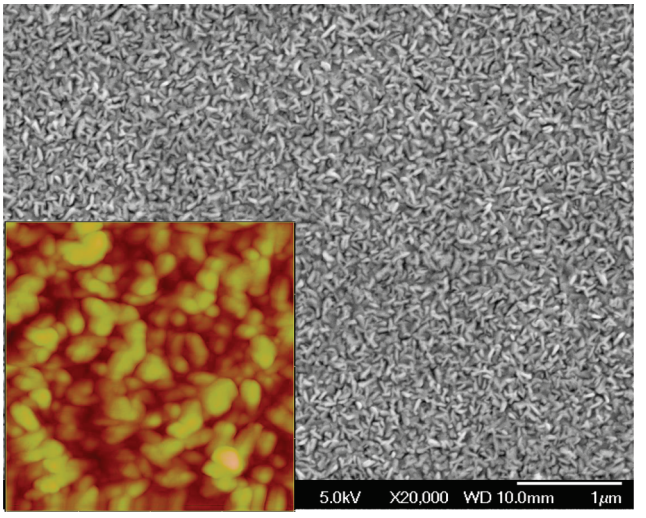

Figure 7. FESEM image of the Mo_2C film morphology. Inset —AFM image of a 1 × 1 μm area from within this region.

weak but distinct peaks at BE = 530.4 and 532.9 eV, respectively. It is speculated that the former is due to molybdenum oxide, whereas the latter may arise from chemisorbed CO, which is a major impurity in the industrial grade N_2 that is used during cooling before. Note that is practice, this residual oxide would be removed by reduction prior to their use as catalysts.

XPS was also used to examine the nature of carbon bonding in the carburized film. In studies of molybdenum carbide, including both powder and thin film form, graphitic carbon is often found to co-exist with Mo_2C. For example, high-resolution transmission electron microscopy has revealed that both carbide powders and films display nanocrystalline domains coated with thin layers of amorphous, graphitic carbon.[3,9] In this work XPS was performed ex situ, and there is always concern about distinguishing carbon germane to the sample from contamination that is present on all samples. Figure 6 contains high-resolution spectra from the C 1s region. The bottom spectrum is from an as-deposited molybdenum oxide film, which displays the adventitious C signal common to all samples. A sputter treatment was developed to fully remove this layer (middle scan). The top spectrum was obtained from a carbide film subjected to the identical sputter treatment. The signal is dominated by a Gaussian signal positioned at BE = 283.2 eV, the position of which is in good agreement with the literature reports of the carbide phase (Table I).[4,25,26,30] There is also a small shoulder at higher binding energy, suggesting the presence of a small amount of graphitic carbon in the sample.

Finally, the morphology of the films was studied by FESEM and AFM. The as-deposited oxide films were smooth and featureless, as one would expect for an amorphous material. Figure 7 displays FESEM and AFM images taken from a carburized film. The images reveal a nanostructured surface, with individual crystal sizes on the order of 50−100 nm. The RMS roughness of the films was ∼11 nm, an order magnitude greater

than the as-deposited oxides. As with unsupported catalysts, the details of the nanostructure are expected to be critical to the catalytic properties of the resulting films. Likewise, it expected that the resulting nanostructure may be modified by TPR parameters (ramp rate, % hydrocarbon, etc.),[1−4] and studies are underway to examine these effects on the thin film morphology and relate them to catalyst performance.

The evidence presented above demonstrates that the two-stage process described within has the ability to produce phase pure β-Mo_2C in a thin film form. This is a distinct advantage over previous attempts to synthesize molybdenum carbide films directly through vapor deposition processes. For example, thermal CVD at 800 °C produced primarily mixtures of off-stoichiometric MoC_{1-x} phases.[14] Films deposited by PECVD films were found to be carbon-rich, with a substantial amount of impurities present.[8] Composition control has also been problematic in efforts to form molybdenum carbide by co-sputtering.[10,11] In these vapor-phase techniques, the resulting film composition is most likely controlled by the kinetics of Mo and C incorporation. In contrast, the use of oxide film growth in conjunction with the slow TPR process favors the formation of thermodynamically stable phases.[2]

CONCLUSIONS

A two-step approach was introduced for the fabrication of β-Mo_2C thin films. First, it was shown that dense molybdenum oxide films could be readily deposited using mixtures of MoF_6/H_2/O_2 at room temperature. The amorphous oxide films contained no detectable impurities and displayed high refractive indices. These films were successfully converted into β-Mo_2C using temperature-programmed reaction in CH_4/H_2. The phase and compositional purity of the resulting films was confirmed by XRD and XPS. The resulting films display a nanostructured morphology, and investigations are underway to assess their performance as hydrogen dissociation catalysts.

AUTHOR INFORMATION

Corresponding Author
*E-mail: cwolden@mines.edu.

ACKNOWLEDGMENT

We gratefully acknowledge support for this work provided by Department of Energy's National Energy Technology Laboratory through contract DE-FE0001009 and the National Renewable Energy Laboratory through task order agreement KXEA-3-33607-47.

REFERENCES

(1) Lee, J. S.; Oyama, S. T.; Boudart, M. *J. Catal.* **1987**, *106*, 125–133.
(2) Oyama, S. T. *Catal. Today* **1992**, *15*, 179–200.
(3) Hanif, A.; Xiao, T.; York, A. P. E.; Sloan, J.; Green, M. L. H. *Chem. Mater.* **2002**, *14*, 1009–1015.
(4) Oshikawa, K.; Nagai, M.; Omi, S. *J. Phys. Chem. B* **2001**, *105*, 9124–9131.
(5) Rebrov, E. V.; Kuznetsov, S. A.; de Croon, M. H. J. M.; Schouten, J. C. *Catal. Today* **2007**, *125*, 88–96.
(6) Dubrovskiy, A. R.; Rebrov, E. V.; Kuznetsov, S. A.; Schouten, J. C. *Catal. Today* **2009**, *147*, S198–S203.
(7) Koós, Á.; Solymosi, F. *Catal. Lett.* **2010**, *138*, 23–27.
(8) Yoon, S. F.; Huang, Q. F.; Rusli; Yang, H.; Ahn, J.; Zhang, Q.; Blomfield, C.; Tielsch, B.; Tan, L. Y. C. *J. Appl. Phys.* **1999**, *86*, 4871–4875.
(9) Koutzaki, S. H.; Krzanowski, J. E.; Nainaparampil, J. J. *Metallurg. Mater. Trans. A* **2002**, *33*, 1579–1588.
(10) De Temmerman, G.; Ley, M.; Boudaden, J.; Oelhafen, P. *J. Nucl. Mater.* **2005**, *337*, 956–959.
(11) Tripathi, C. C.; Kumar, M.; Kumar, D. *Appl. Surf. Science* **2009**, *255*, 3518–3522.
(12) Leroy, W. P.; Detavernier, C.; Van Meirhaeghe, R. L.; Kellock, A. J.; Lavoie, C. *J. Appl. Phys.* **2006**, *99*, 063704.
(13) Bagge-Hansen, M.; Outlaw, R. A.; Miraldo, P.; Zhu, M. Y.; Hou, K.; Theodore, N. D.; Zhao, X.; Manos, D. M. *J. Appl. Phys.* **2008**, *103*, 014311.
(14) Lu, J.; Hugosson, H.; Eriksson, O.; Nordström, L.; Jansson, U. *Thin Solid Films* **2000**, *370*, 203–212.
(15) Kuznetsov, S. A.; Dubrovskiy, A. R.; Rebrov, E. V.; Schouten, J. C. *Z. Naturforsch., A: Phys. Sci.* **2007**, *62*, 647–654.
(16) Kitchin, J. R.; Norskov, J. K.; Barteau, M. A.; Chen, J. G. G. *Catal. Today* **2005**, *105*, 66–73.
(17) Tracy, C. E.; Benson, D. K. *J. Vac. Sci. Technol., A* **1986**, *4*, 2377–2383.
(18) Cross, J. S.; Schrader, G. L. *Thin Solid Films* **1995**, *259*, 5–13.
(19) Juppo, M.; Vehkamaki, M.; Ritala, M.; Leskela, M. *J. Vac. Sci. Technol., A* **1998**, *16*, 2845–2850.
(20) Seman, M.; Wolden, C. A. *J. Vac. Sci. Technol., A* **2003**, *21*, 1927–1933.
(21) Fleisch, T. H.; Mains, G. J. *J. Chem. Phys.* **1982**, *76*, 780–786.
(22) Otterman, C. R.; Bange, K.; Wagner, W.; Laube, M.; Rauch, F. *Surf. Interface Anal.* **1992**, *19*, 435.
(23) Abdellaoui, A.; Leveque, G.; Donnadieu, A.; Bath, A.; Bouchikhi, B. *Thin Solid Films* **1997**, *304*, 39–44.
(24) Briggs, D.; Seah, M. P., Eds.; John Wiley and Sons: Chichester, U.K., 1983.
(25) Reinke, P.; Oelhafen, P. *Surf. Sci.* **2000**, *468*, 203–215.
(26) Weigert, E. C.; Esposito, D. V.; Chen, J. G. *J. Power Sources* **2009**, *193*, 501–506.
(27) Ivanova, T.; Gesheva, K. A.; Popkirov, G.; Ganchev, M.; Tzvetkova, E. *Mater. Sci. Eng. B* **2005**, *119*, 232–239.
(28) Wu, H. H.; Chen, J. G. *Chem. Rev.* **2005**, *105*, 185–212.
(29) Spevack, P. A.; McIntyre, N. S. *J. Phys. Chem.* **1993**, *97*, 11020–11030.
(30) Lu, J.; Jansson, U. *Thin Solid Films* **2001**, *396*, 53–61.